(7) Micheloni, M.; Sabatini, A.; Vacca, A. *Inorg. Chim. Acta* **1977**, *25*, 41.
(8) Sabatini, A.; Vacca, A.; Gans, P. *Talanta* **1974**, *21*, 53.
(9) Ivaroska, I.; Bleha, T. *Biopolymers* **1979**, *18*, 2537.
(10) Malrieu, J. P. *Mod. Theor. Chem.* **1977**, *7*, 69.
(11) Pullman, A.; Port, G. N. J. *Theor. Chim. Acta* **1973**, *32*, 77.
(12) (a) Barone, V.; Lelj, F.; Russo, N. *Mol. Pharmacol.* **1980**, *18*, 331. (b) Barone, V.; Lelj, F.; Russo, N.; Gemelli, M. L. *Gazzetta*, in press.
(13) Pullman, B.; Maigret, B. In "Conformation of Biological Molecules and Polymers"; Bergman, B., Pullman, B., Eds.; Academic Press: New York, 1973.
(14) IUPAC–IUB Commission of Biochemical Nomenclature *Eur. J. Biol.* **1970**, *17*, 193. IUPAC Commission on Macromolecular Nomenclature *Pure Appl. Chem.* **1974**, *40*, 479. IUPAC Commission on Organic Nomenclature *Ibid.* **1975**, *41*, 123.
(15) (a) Pople, J. A.; Gordon, M. *J. Am. Chem. Soc.* **1967**, *89*, 4253. (b) Scheraga, H. A. *Adv. Phys. Org. Chem.* **1968**, *6*, 103.
(16) Barbucci, R.; Paoletti, P.; Vacca, A. *J. Chem. Soc. A* **1970**, 2202.
(17) Christensen, J. J.; Izatt, R. M.; Wrathal, D. P.; Hansen, L. D. *J. Chem. Soc. A* **1969**, 1212.
(18) Barbucci, R.; Ferruti, P.; Micheloni, M.; Delfini, M.; Segre, A. L.; Conti, F. *Polymer* **1980**, *21*, 81.
(19) Bloys, C. J.; van Treslong, E. *Recl. Trav. Chim. Pays-Bas* **1978**, *1*, 97. Puterman, M.; Garcia, E.; Lando, J. B. *J. Macromol. Sci.* **1979**, *B16* (1), 117. Marina, M. G.; Monakov, Yu. B.; Rafikov, S. R. *Russ. Chem. Rev.* **1979**, *48*, 389.
(20) Batchelor, J. G.; Feeney, J.; Roberts, G. C. K. *J. Magn. Reson.* **1975**, *20*, 19. Marishima, I.; Yoshinawa, K.; Okada, K.; Yonezawa, T.; Goto, G. *J. Am. Chem. Soc.* **1973**, *95*, 165.
(21) (a) Barone, V.; Del Re, G.; Fliszar, S. *J. Chem. Soc., Perkin Trans. 2* **1979**, 1309. (b) Barbucci, R.; Barone, V. *J. Solution Chem.* **1979**, *8*, 427.
(22) Barbucci, R.; Ferruti, P.; Improta, C.; La Torraca, M.; Oliva, L.; Tanzi, M. C. *Polymer* **1979**, *20*, 1298.

Length Distributions and the Alignment Transition of Polymers Formed by Linear Reversible Polymerization

Judith Herzfeld* and Robin W. Briehl

Biophysical Laboratory, Harvard Medical School, Boston, Massachusetts 02115, and the Departments of Biochemistry and Physiology, Albert Einstein College of Medicine, Bronx, New York 10461. *Received January 8, 1981*

ABSTRACT: The equilibrium distributions of polymer lengths and orientations are calculated for reversible linear polymerization, assuming that the free energy of monomer addition is independent of polymer size. The anisotropy of the equilibrium state at high concentrations has two aspects. (1) In the absence of anisotropy in the interactions between molecules, the system is isotropic with respect to monomer orientation, but the average polymer length is greater along the axis of alignment than orthogonal to it. (2) In the presence of anisotropic interactions between molecules, the orientation of monomers is also anisotropic. The phase diagram differs somewhat from that calculated earlier for an approximation of a reversibly polymerizing system in which all the polymers were constrained to be of identical, albeit reversibly changeable, length. In particular, noninteracting polymers do not form as dense an anisotropic phase as was predicted earlier. However, the temperature dependence of the phase behavior of the present freely reversible system and that of the former constrained reversible system are qualitatively similar to one another and qualitatively distinct from that of irreversibly polymerized systems. In particular, there exists for the reversibly polymerized systems, in contrast to the irreversibly polymerized systems, a temperature below which, for positive enthalpies of polymerization, or above which, for negative enthalpies of polymerization, no phase transition occurs. The maximum concentration of the isotropic phase is found to depend primarily on the free energy of polymerization, to be relatively insensitive to the nature of interparticle interactions, and to have a temperature dependence which is qualitatively similar to that observed for sickle cell hemoglobin. The distribution of polymer lengths in the isotropic phase is significantly different from that observed for sickle cell hemoglobin, presumably due to the relative instability of subnuclear hemoglobin aggregates which is not incorporated into the present model. The minimum concentration of the anisotropic phase is found to depend strongly on both the free energy of polymerization and the interparticle interactions and, in general, has a complicated temperature dependence.

Introduction

A variety of proteins associate reversibly to form long polymers. Among these are tubulin, actin and actin-like proteins, tobacco mosaic virus protein, and sickle cell hemoglobin. The excluded volume dependent nonideality associated with the highly asymmetric shapes of such polymers can induce spontaneous alignment and phase separation. This phenomenon is entropically driven; it is modified by, but not dependent upon, the nature of the interparticle interactions.[1]

Lattice models for monodipserse hard rods[2,3] have successfully explained the main features of the observed phase behavior of α-helical polypeptides[4-9] and *p*-phenylene polyamides.[10-13] Such synthetic systems are relatively simple to describe because the polymer length is fixed and the approach to equilibrium involves adjustment of polymer orientation only. In contrast, proteins form polymers which may reversibly change length so that equilibration involves the joint optimization of polymer lengths and orientations. The lattice models of Flory[2] and DiMarzio[3] have previously been used to describe reversibly polymerizing systems by assuming a narrow length distribution.[14,15] Thus, the number of degrees of freedom in the approach to equilibrium was limited to two (average polymer length and average polymer orientation) by imposing the constraint that the polymers were of uniform, albeit adjustable length. We will hereafter refer to this as constrained reversible polymerization. In the present treatment, based on DiMarzio's lattice model, this artificiality is removed and no constraints whatever are placed on the polymer lengths. It is therefore possible to calculate the expected equilibrium *distribution* of lengths, as well

* To whom correspondence should be addressed at Harvard Medical School.

0024-9297/81/2214-1209$01.25/0

as orientations. Some of the results, derived in detail here, have been presented in a summary way previously.[16]

Partition Function

In DiMarzio's simplest model, each molecule is assumed to lie in the direction of one of three mutually perpendicular axes of a simple cubic lattice.[3] Such restriction to a few discrete orientations may tend to exaggerate alignment.[17] However, the phase behavior predicted with this model[15] has the same qualitative features as that predicted by Flory's lattice model which allows a continuum of particle orientations.[14] DiMarzio's model has the advantage, for our purposes, of readily incorporating an arbitrary degree of polydispersity.

In the lattice model, the statistics for arranging rodlike particles, of axial ratio x, in space is computed by dividing the particles along their length into x equal cubic segments and counting the number of ways in which these segments can be packed into a lattice of cells of the same size. It has been noted[19] that the number of ways of arranging a collection of rodlike particles in a given orientation on a lattice depends on the total number of segments and the number of these which are end segments, or, alternatively, the number of particles and their average axial ratio. Thus, generalizing from DiMarzio's[3] eq 7, the number of ways, g, of arranging a polydisperse collection of rods on a lattice, in three mutually orthogonal orientations (i = 1, 2, 3), depends on the average length ($\bar{x}_i$) and number of rods ($\bar{N}_i$) in each direction according to the equation

$$g = \frac{1}{S}\frac{\prod_{i=1}^{3}(N - \bar{x}_i N_i + N_i)!}{N!^2(N - \bar{x}_1N_1 - \bar{x}_2N_2 - \bar{x}_3N_3)!} \tag{1}$$

where N is the total number of lattice cells and S is the statistical factor that corrects for multiple counting of arrangements which are identical due to indistinguishability of particles. If N_{ix} is the number of rods of length x in direction i, then

$$N_i = \sum_{x=1}^{\infty} N_{ix} \tag{2}$$

$$\bar{x}_i = \sum_{x=1}^{\infty} xN_{ix}/N_i \tag{3}$$

and

$$S = \prod_{i=1}^{3}\prod_{x=1}^{\infty} N_{ix}! \tag{4}$$

Using Stirling's approximation

$$\ln g = N\left\{\sum_{i=1}^{3}\left[g_i \ln g_i - \sum_{x=1}^{\infty}\left(\frac{N_{ix}}{N}\right)\ln\left(\frac{N_{ix}}{N}\right)\right] - (1 - v)\ln(1 - v)\right\} \tag{5}$$

Here

$$g_i = 1 - (\bar{x}_i - 1)N_i/N = 1 - \sum_{x=1}^{\infty}(x - 1)N_{ix}/N \tag{6}$$

and v is the total volume fraction of solute

$$v = \frac{1}{N}\sum_{i=1}^{3}\sum_{x=1}^{\infty} xN_{ix} = \sum_{i=1}^{3}\bar{x}_iN_i/N \tag{7}$$

To compute the partition function, it is also necessary to incorporate polymerization interactions and rod–rod interactions. Assuming linear polymerization, with only one type of linkage, the number of linkages is

$$\sum_{i=1}^{3}\sum_{x=1}^{\infty}(x - 1)N_{ix} = \sum_{i=1}^{3}(\bar{x}_i - 1)N_i \tag{8}$$

Assuming a random spatial distribution of polymers in any given direction, the number of parallel contacts between rods is

$$(1/2)\sum_{i=1}^{3}(\bar{x}_iN_i)(\bar{x}_iN_i)/N \tag{9a}$$

and the number of perpendicular contacts between rods is

$$(1/2)\sum_{\substack{i=1\\ i\neq j}}^{3}\sum_{j=1}^{3}(\bar{x}_iN_i)(\bar{x}_jN_j)/N \tag{9b}$$

The partition function may then be expressed as

$$Z = \sum_{\substack{\text{all config}\\ \{N_{ix}\}}} \exp(-Nf/kT) \tag{10}$$

where

$$f = -\left(\frac{1}{N}\right)\ln g + \phi\sum_{i=1}^{3}(\bar{x}_i - 1)\left(\frac{N_i}{N}\right) + \left(\frac{w_\parallel}{2}\right)\sum_{i=1}^{3}\left(\frac{\bar{x}_iN_i}{N}\right)^2 + \left(\frac{w_\perp}{2}\right)\sum_{\substack{i=1\\ i\neq j}}^{3}\sum_{j=1}^{3}\left(\frac{\bar{x}_iN_i}{N}\right)\left(\frac{\bar{x}_jN_j}{N}\right) \tag{11}$$

ϕ is the free energy of formation of each polymer linkage, and $w_\parallel$ and $w_\perp$ are the energies of interaction between rods per parallel and perpendicular contact, respectively. Notice that the expression that we have adopted for the rod–rod interaction energy[18] embodies the assumption that rod segments interact strictly pairwise. This approximation is expected to be poor at high densities. However, as discussed below, our results suggest that the detailed form of the rod–rod interaction energy is relatively unimportant because the phase behavior is more sensitive to polymerization interactions than to the rod–rod interactions.

Applying the maximum term approach, the equilibrium state is that state $\{N_{ix}\}$ for which f attains the minimum value $\tilde{f}$, for given values of v, ϕ, $w_\parallel$, and $w_\perp$. Then $\tilde{f}$ is the free energy per lattice cell of the system at equilibrium and the chemical potentials of solvent and solute are, respectively,

$$\mu_1 = RT\{\tilde{f} - v(\partial\tilde{f}/\partial v)\} \tag{12a}$$

and

$$\mu_2 = RT\{\tilde{f} + (1 - v)(\partial\tilde{f}/\partial v)\} \tag{12b}$$

The Equilibrium State

It is convenient to define a new set of variables

$$C_{ix} = N_{ix}/N \tag{13}$$

in terms of which

$$f = \sum_{i=1}^{3}\left[-g_i \ln g_i + \sum_{x=1}^{\infty} C_{ix}\ln C_{ix} + \phi\sum_{x=1}^{\infty}(x - 1)C_{ix} + \left(\frac{w_\parallel - w_\perp}{2}\right)\left(\sum_{x=1}^{\infty} xC_{ix}\right)^2\right] + \left(\frac{w_\perp}{2}\right)\left(\sum_{i=1}^{3}\sum_{x=1}^{\infty} xC_{ix}\right)^2 + (1 - v)\ln(1 - v) \tag{14}$$

and

$$g_i = 1 - \sum_{x=1}^{\infty}(x - 1)C_{ix} \tag{15}$$

Our goal then is to find the minimum of f with respect to

all the C_{ix}, subject to the condition that

$$\sum_{i=1}^{3}\sum_{x=1}^{\infty} xC_{ix} = v \tag{16}$$

In light of this constraint, eq 14 may be rewritten as

$$f = \sum_{i=1}^{3}\left[-g_i \ln g_i + \sum_{x=1}^{\infty} C_{ix} \ln C_{ix} + \phi\sum_{x=1}^{\infty}(x-1)C_{ix} + \left(\frac{w_\parallel - w_\perp}{2}\right)\left(\sum_{x=1}^{\infty} xC_{ix}\right)^2\right] + \left(\frac{w_\perp}{2}\right)v^2 + (1-v)\ln(1-v) \tag{17}$$

The method of Lagrange multipliers requires that the extrema of f satisfy the equations

$$\lambda x = \partial f/\partial C_{ix} = \ln C_{ix} + x + (x-1)\ln g_i + (x-1)\phi + (w_\parallel - w_\perp)x\sum_{x'=1}^{\infty} x'C_{ix'} \tag{18}$$

for all i and x, in addition to eq 16. Thus

$$C_{i1} = \exp(\lambda - 1)/\exp[(w_\parallel - w_\perp)\sum_{x=1}^{\infty} xC_{ix}] \tag{19}$$

and

$$C_{ix} = (z_i)^{x-1}C_{i1} \tag{20a}$$

where

$$z_i = C_{i1}e^{-\phi}/g_i \tag{20b}$$

Notice, with regard to eq 19 that when $w_\parallel = w_\perp$, $C_{11} = C_{21} = C_{31}$, indicating, as expected under these conditions, that there is no preferred orientation for monomers. From the relationships

$$\sum_{x=1}^{\infty} xz^{x-1} = (1-z)^{-2} \tag{21a}$$

and

$$\sum_{x=1}^{\infty} z^{x-1} = (1-z)^{-1} \tag{21b}$$

it follows from eq 20a that

$$\sum_{x=1}^{\infty} xC_{ix} = C_{i1}(1-z_i)^{-2} \tag{22a}$$

and

$$\sum_{x=1}^{\infty} C_{ix} = C_{i1}(1-z_i)^{-1} \tag{22b}$$

so that from eq 3 and 13

$$\bar{x}_i = (1-z_i)^{-1} \tag{22c}$$

from eq 15

$$g_i = 1 - C_{i1}z_i(1-z_i)^{-2} \tag{22d}$$

from eq 19

$$\exp(\lambda - 1) = C_{i1}\exp[(w_\parallel - w_\perp)C_{i1}(1-z_i)^{-2}] \tag{23}$$

for all i, and from eq 16

$$v = \sum_{i=1}^{3} C_{i1}(1-z_i)^{-2} \tag{24}$$

Combining eq 20b and 22d gives

$$C_{i1}^{-1} = e^{-\phi}/z_i + z_i(1-z_i)^{-2} \tag{25}$$

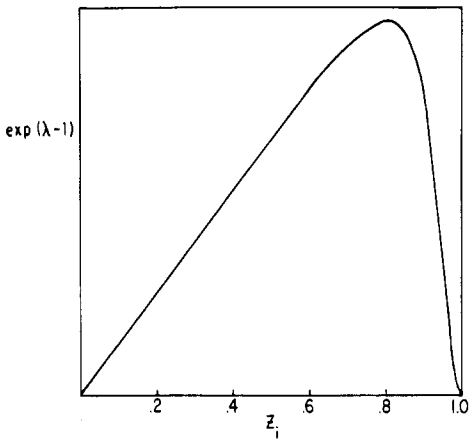

Figure 1. Right-hand side of eq 26 plotted as a function of z_i for $\phi = -5.0$ and $w_\parallel - w_\perp = 0$, showing that z_i is at most a double-valued function of λ.

Substituting eq 25 into eq 23 and 24, we find that, for the extrema of f, the z_i satisfy the equations

$$\exp(\lambda - 1) = \left[\frac{z_i(1-z_i)^2}{e^{-\phi}(1-z_i)^2 + z_i^2}\right]\exp\left[\frac{(w_\parallel - w_\perp)z_i}{e^{-\phi}(1-z_i)^2 + z_i^2}\right] \tag{26}$$

for all i, and

$$v = \sum_{i=1}^{3}\frac{z_i}{e^{-\phi}(1-z_i)^2 + z_i^2} \tag{27}$$

The C_{ix} are then given by eq 25 and 20a.

As shown in Figure 1, there are no more than two different values of z_i which satisfy eq 26 for any given value of λ. Therefore, two of the three directions in the lattice must be equivalent; if we choose z_1 to be unique, then $z_2 = z_3$. Due to this symmetry, it is possible to define a convenient measure of alignment of solute as

$$y = \frac{\sum_{x=1}^{\infty} xN_{1x}}{\sum_{i=1}^{3}\sum_{x=1}^{\infty} xN_{ix}} = \frac{\sum_{x=1}^{\infty} xC_{1x}}{\sum_{i=1}^{3}\sum_{x=1}^{\infty} xC_{ix}} = \left(\frac{1}{v}\right)\left[\frac{z_1}{e^{-\phi}(1-z_1)^2 + z_1^2}\right] \tag{28}$$

which varies from 1, for perfect axial alignment, to $^1/_3$, for an isotropic distribution, to 0, for a fully planar array.

Figure 2 shows the loci of the solutions of eq 26 in the z_1, $z_2 = z_3$ plane, for various values of ϕ. Trivial solutions occur along the line $z_1 = z_2 = z_3$ corresponding to isotropic states. In addition, there is a branch of solutions corresponding to axial alignment ($z_1 > z_2 = z_3$) and a branch corresponding to planar arrays ($z_1 < z_2 = z_3$). Figure 3 shows the loci of the solutions of eq 27 for various values of v and ϕ. Local extrema in f occur at the points where the loci of Figures 2 and 3 cross, for given values of $w_\parallel - w_\perp$, ϕ, and v. There is always at least one extremum at

$$z_1 = z_2 = z_3 = \frac{2e^{-\phi}v + 3 - [9 + 4e^{-\phi}v(3-v)]^{1/2}}{v[2e^{-\phi} + 2]} \tag{29}$$

For low values of v there are no other extrema. For high values of v there are, in addition, one axial extremum and one planar extremum, which we locate numerically by repeated bisection on either side of the isotropic extremum. Over a very narrow range of intermediate values of v, there are two axial extrema and no planar extrema. One of these axial extrema is located numerically by iteration between

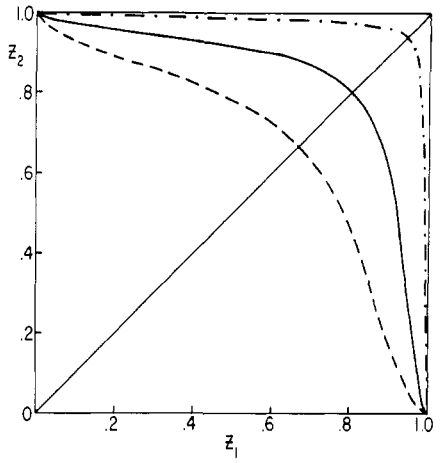

Figure 2. Loci of solutions of eq 26 for $w_{\parallel} - w_{\perp} = 0$ and $\phi = -3.0$ (– – –), −5.0 (——), and −9.0 (·–·).

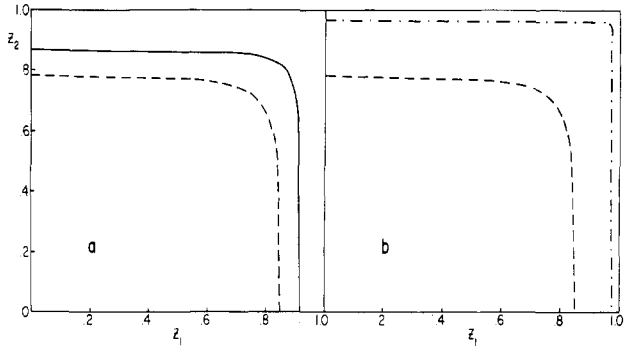

Figure 3. Loci of the solutions of eq 27 for (a) $\phi = -5.0$ and $v = 0.2$ (– – –) and 0.5 (——) and (b) $v = 0.2$ and $\phi = -5.0$ (– – –) and −9.0 (·–·).

the two loci, starting at the isotropic extremum, and the other is then located by repeated bisection.

For each of the local extrema, f is evaluated according to eq 17, 22d, 25, and 20a, in order to determine which corresponds to the absolute minimum in f and the equilibrium state. Figure 4 shows the dependence of the equilibrium values of the alignment parameter, the average rod lengths in each direction, and the monomer concentrations in each direction on v, for $w_{\parallel} - w_{\perp} = 0$ and various values of ϕ. At low values of v, the system is isotropic: $\bar{x}_1 = \bar{x}_2 = \bar{x}_3$ and $y = {}^1/_3$. In this region, the monomer concentration increases less rapidly than the total concentration of solute, corresponding to the appreciable formation of polymer indicated by the increasing average polymer length. The more negative the value of ϕ, the lower the monomer concentration and the greater the average rod length. At higher values of v, the system becomes anisotropic: the average rod length along the unique axis ($\bar{x}_1$) increases, and the average rod length along the two equivalent axes ($\bar{x}_2$, $\bar{x}_3$) decreases, with increasing v. This corresponds to strong axial alignment, as indicated by the abrupt increase in y. The overall average rod length

$$\begin{aligned} \bar{x} &= \sum_{i=1}^{3} \sum_{x=1}^{\infty} x N_{ix} / \sum_{i=1}^{3} N_i \\ &= \sum_{i=1}^{3} \bar{x}_i N_i / \sum_{i=1}^{3} N_i \\ &= \bar{x}_1 y + \bar{x}_2 (1 - y) \end{aligned} \tag{30}$$

also increases rapidly, until $\bar{x} \cong \bar{x}_1$ when $y \cong 1$. In addition, the monomer concentration decreases, with increasing v, due to the increasing anisotropy of the average polymer length.

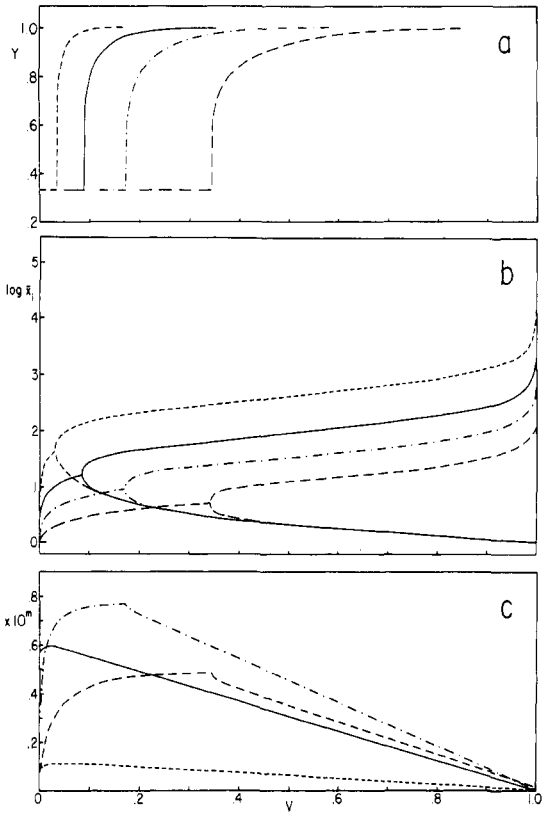

Figure 4. Dependence on v of the equilibrium values of (a) the orientation parameter (eq 28), (b) the average polymer lengths (eq 22c), and (c) the monomer concentrations (eq 25) for $w_{\parallel} - w_{\perp} = 0$ and $\phi = -5.0$, $m = 2$ (– – –), $\phi = -7.0$, $m = 3$ (·–·), $\phi = -9.0$, $m = 3$ (——), and $\phi = -12.0$, $m = 5$ (– · –).

Phase Behavior

Using the equilibrium values of z in each direction, one can calculate the chemical potentials of the solute and solvent as functions of v, according to eq 12a,b. A discontinuity in the chemical potential occurs at the alignment transition and phase separation occurs between the two ends of the corresponding van der Waals loop. Figure 5 shows the dependence of the composition of the coexisting isotropic and anisotropic phases on $w = w_{\parallel} = w_{\perp}$ and ϕ. In these phase diagrams, a single isotropic phase occurs in the left-most area, the conjugate isotropic and anisotropic phases coexist in the middle area, and a single anisotropic phase occurs in the right-most area. Like the corresponding phase diagrams for irreversible polymerization and constrained reversible polymerization (see Figure 3 of ref 15), the form of the diagram in Figure 5a is stemlike: in the region of strong repulsion between rods ($w \gg 0$), the two-phase region is narrow, the coexisting isotropic and anisotropic phases differing relatively little in concentration; in the region of strong attraction between rods ($w \ll 0$), the two-phase region is very wide, a very dilute isotropic phase coexisting with a very dense and highly aligned anisotropic phase. As in the case for irreversible polymerization, and contrary to the case for constrained reversible polymerization, the "shoulder" (i.e., the change from a narrow to a wide two-phase region) occurs in the range of attractive interactions ($w < 0$). As is the case for irreversible polymerization, and contrary to the situation for constrained reversible polymerization, the "shoulder" may be humped so that in a narrow portion of the attractive region ($w < 0$) two distinct phase transitions may occur (as, for example, when $\phi = -12$ in Figure 5a). In all cases, the position of the isotropic boundary of the two-phase region is only weakly dependent on w. On the

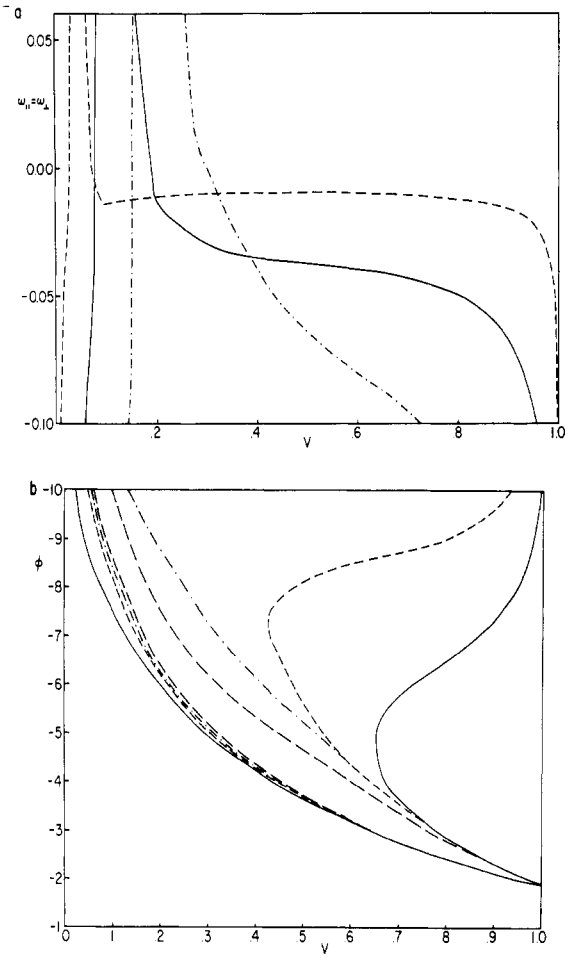

Figure 5. Dependence of the phase boundaries on (a) the interactions between polymers for ϕ = -7.0 (·–·), -9.0 (——), and -12.0 (– – –) and (b) the free energy of polymerization for $w_\parallel$ = $w_\perp$ = -0.15 (——), -0.05 (- - -), 0.00 (·–·), and +0.15 (– – –).

other hand, it is very strongly dependent on rod length in the irreversibly polymerized system and on the free energy of polymerization, ϕ, in the reversibly polymerized system. In all cases, the position of the anisotropic boundary is weakly dependent on w above and below the "shoulder", but is strongly dependent on w in the vicinity of the shoulder. It is also strongly dependent on rod length in the irreversibly polymerized system and on the free energy of polymerization in the reversibly polymerized system.

Temperature Dependence

Thus far it appears that the results for unconstrained reversible polymerization bear closer resemblance to the results for irreversible polymerization than to those for constrained reversible polymerization. However, a great distinction between the reversibly and irreversibly polymerized systems is seen in the temperature dependence. Because the rod length in the irreversibly polymerized system is independent of temperature, the phase behavior of this system is determined solely by the temperature dependence of w. In contrast, the free energy of polymerization in the reversibly polymerized systems is dependent on temperature, and the phase behavior is determined by the temperature dependence of both ϕ and w. In fact, the dependence on ϕ is much stronger than than on w, except for the "shoulder" in the anisotropic boundary. Thus, whereas for irreversible polymerization the temperature phase diagram will be of the stemlike form shown in Figure 5a, for reversible polymerization (constrained or unconstrained) the predicted temperature

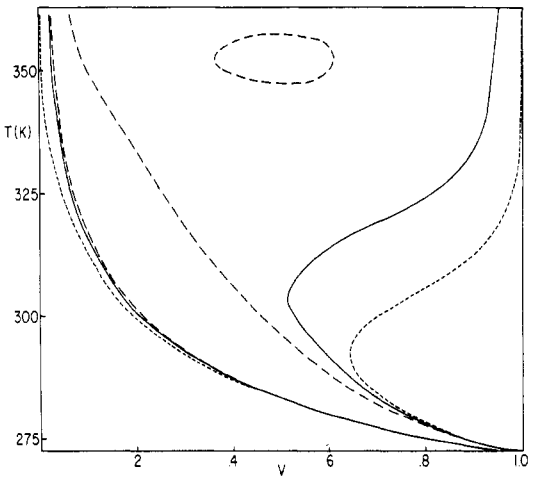

Figure 6. Temperature phase diagrams for $\phi = (12000/T) - 46$ and $w_\parallel = w_\perp = 0.32 - (120/T)$ (——), $0.16 - (60/T)$ (– – –), and $0.06 - (60/T)$ (- - -).

phase diagram will be of the elbowlike form shown in Figure 5b.

The latter phase behavior is illustrated in Figure 6 for various simple hypothetical functions for the temperature dependence of ϕ and w (to compare with Figures 5 and 7 of ref 15). We have chosen positive enthalpies of polymerization because protein polymerization is usually endothermic. For reversible polymerization (constrained or unconstrained), unlike irreversible polymerization, there exists a temperature below which no phase transition occurs. Above that temperature, the concentration of the isotropic conjugate phase decreases with increasing temperature, at a rate which also decreases with increasing temperature, to give an elbow-shaped boundary. The corresponding concentration of the anisotropic phase depends strongly on the temperature dependence of the interactions between rods.

Sickle Cell Hemoglobin

At sufficiently high temperatures and concentrations, sickle cell hemoglobin forms a two-phase system in which birefringent bodies coexist with an isotropic solution. Rapid ultracentrifugation sediments the birefringent bodies and the temperature dependence of the supernatant concentration has the same elbow-like form seen in Figures 5b and 6.[20-24] However, it is not known whether the supernatant truly reflects the composition of the isotropic conjugate phase. In the present model, the isotropic phase is predicted to contain some polymers large enough to be sedimented along with the birefringent bodies. In addition, polymers that are too small to be sedimented at these speeds are predicted to be present at concentrations comparable to the monomer concentration. Since the latter prediction is inconsistent with the experimental observation that hemoglobin in the supernatant consists nearly exclusively of monomers, the former prediction is also suspect for this system.

The theoretically predicted size distribution is a direct consequence of the assumption that polymerization occurs with only one type of linkage (i.e., by a head-to-tail association of monomers), so that the free energy of addition of a monomer to a growing polymer is independent of polymer length. However, in sickle cell hemoglobin, and in other tubule-forming proteins, the free energy of addition of the first few units is probably much higher than that for subsequent addition. This would result in depression of the population of small polymers. Thus, the absence of small polymers in the isotropic phase may be

an equilibrium reflection of the nucleation process seen in kinetics experiments.[24,25] Since nucleation kinetics also produces transient length overshoot, the absence of small polymers in the supernatant may also be partially due to incomplete equilibration. We are presently calculating the equilibrium distributions of polymer sizes and orientations, and the corresponding phase diagrams, for nucleated reversible polymerization. It is anticipated that the behavior will be intermediate between that for unconstrained reversible polymerization, as presented here, and constrained reversible polymerization in which monomer and polymer do not coexist in significant amounts in the same phase, as presented previously.[14,15]

Acknowledgment. We thank Irene Mendelson for assistance with computing. This work was supported by U.S. Public Health Service Grants AM21077 and HL07451. J.H. is supported by a Faculty Research Award from the American Cancer Society and NIH Grant RR05381.

References and Notes

(1) Onsager, L. *Ann. N.Y. Acad. Sci.* **1949**, *51*, 627–59.
(2) Flory, P. J. *Proc. R. Soc. London, Ser. A* **1956**, *234*, 73–89.
(3) DiMarzio, E. A. *J. Chem. Phys.* **1961**, *35*, 658–69.
(4) Robinson, C. *Trans. Faraday Soc.* **1956**, *52*, 571–92.
(5) Hermans, J. *J. Colloid Sci.* **1962**, *17*, 638–48.
(6) Nakajima, A.; Hayashi, T.; Ohmori, M. *Biopolymers* **1968**, *6*, 973–82.
(7) Wee, E. L.; Miller, W. G. *J. Phys. Chem.* **1971**, *75*, 1446–52.
(8) Miller, W. G.; Wu, C. C.; Wee, E. L.; Santee, G. L.; Rai, J. H.; Goebel, K. G. *Pure Appl. Chem.* **1974**, *37*, 37–58.
(9) Miller, W. G.; Rai, J. H.; Wee, E. L. *Liq. Cryst. Ordered Fluids* **1974**, *2*, 243–55.
(10) Papkov, S. L. *Khim. Volokna* **1973**, *15*, 3.
(11) Papkov, S. P.; Kalichikhin, V. G.; Kalmykova, V. D. *J. Polym. Sci., Polym. Phys. Ed.* **1974**, *12*, 1753–70.
(12) Morgan, P. W. *Polym. Prepr., Am. Chem. Soc., Div. Polym. Chem.* **1976**, *17*, 47–52.
(13) Kwolek, S. L.; Morgan, P. W.; Schaefgen, J. R.; Gulrich, L. W. *Polym. Prepr., Am. Chem. Soc., Div. Polym. Chem.* **1976**, *17*, 53–58.
(14) Briehl, R. W.; Herzfeld, J. *Proc. Natl. Acad. Sci. U.S.A.* **1979**, *76*, 2740–4.
(15) Herzfeld, J.; Briehl, R. W. *Macromolecules* **1981**, *14*, 397–404.
(16) Herzfeld, J.; Briehl, R. W. *Ferroelectrics* **1980**, *30*, 125–32.
(17) Straley, J. P. *J. Chem. Phys.* **1972**, *57*, 3694–5.
(18) Minton, A. P. *J. Mol. Biol.* **1974**, *82*, 483–98.
(19) DiMarzio, E. A.; Gibbs, J. H. *J. Chem. Phys.* **1958**, *28*, 807–13.
(20) Briehl, R. W.; Ewert, S. *J. Mol. Biol.* **1973**, *80*, 445–58.
(21) Ross, P. D.; Hofrichter, J.; Eaton, W. A. *J. Mol. Biol.* **1975**, *96*, 239–56.
(22) Ross, P. D.; Hofrichter, J.; Eaton, W. A. *J. Mol. Biol.* **1977**, *115*, 111–34.
(23) Magdoff-Fairchild, B.; Poillon, W. N.; Li, T.-I.; Bertles, J. F. *Proc. Natl. Acad. Sci. U.S.A.* **1976**, *73*, 990–4.
(24) Hofrichter, J.; Ross, P. D.; Eaton, W. A. In "Proceedings of the Symposium on Molecular and Cellular Aspects of Sickle Cell Disease"; Hercules, J. I., Cottam, G. L., Waterman, M. R., Schechter, A. N., Eds; Department of Health Education and Welfare: Washington, D.C., 1976; Publication No. (NIH) 76-1007, pp 185–222.
(25) Hofrichter, J.; Ross, P. D.; Eaton, W. A. *Proc. Natl. Acad. Sci. U.S.A.* **1974**, *71*, 4864–8.

Configuration Properties of Comb-Branched Polymers

F. L. McCrackin* and J. Mazur

Polymer Science and Standards Division, National Bureau of Standards, Washington, D.C. 20234. *Received December 15, 1980*

ABSTRACT: Mean-square radii of gyration were computed for comb-branched polymers simulated by chains on a cubic lattice that incorporated both excluded volume and attractive energies between nonbounded segments of the polymer. The ratios g of the radius of gyration of comb-branched polymer to that of a linear polymer of the same molecular weight at the Θ point were found to be larger than the g ratios calculated by the unrestricted random walk model of the polymer. The calculated g ratios were compared with experimental measurements. For the comb-branched polymers, the radii of gyration of the backbones and the expansion factors were also calculated. The radii of gyration of the backbones at the Θ conditions were greater than those of linear polymers, in contradiction to the random walk model, which requires that they be equal. The calculated expansion factors were less than those of linear polymers, also in contradiction to perturbation theories based on the random walk model, which predict greater expansion factors for branched polymers than for linear polymers.

Introduction

A branched polymer molecule in solution is less extended than a linear polymer molecule having the same molecular weight. This fact is expressed by the ratio

$$g = \langle s^2 \rangle_b / \langle s^2 \rangle_l < 1 \qquad (1)$$

where $\langle s^2 \rangle_b$ and $\langle s^2 \rangle_l$ are the mean-square radii of gyration, which will be called the squared radii, of branched and linear polymer, respectively.

The most common method of determining the degree of branching of a polymer is to measure its g ratio by light scattering or to infer its value from intrinsic viscosity measurements. From a relationship between the g ratio and the number of branches per molecule for an assumed type of branching (e.g., star, comb, or random), the number of branches is then determined. This relationship is evaluated for comb-branched polymer in this paper.

By representing polymers at the Θ condition as random flight walks, Stockmayer and Zimm obtained the g ratios for branched polymers in a closed form.[1] For randomly branched comb polymers, Casassa and Berry[2] obtained

$$g = (1 + f\rho)^{-3}\{1 + 2f\rho + (2f + f^2)\rho^2 + (3f^2 - 2f)\rho^3\} \qquad (2)$$

where f is the number of branches per molecule and ρ is the ratio of the molecular weight of a branch to that of the backbone. Equation 2 was derived for the case of homogeneous molecular weight of backbone and branches, with a random distribution of branch points on the backbone.

In this paper the g ratios for comb-branched polymers are computed, based on a model that is physically more realistic than the random walk model. In the present model, the branched polymer is simulated by a self-